Electric Machines and Power Systems, 27:465–479, 1999

0731-356X / 99 $12.00 + .00

Adaptive Output Feedback Controller for Wind Turbine Generators Using Neural Networks

H. N. AL-DUWAISH*
Z. M. AL-HAMOUZ*
S. M. BADRAN†

*Department of Electrical Engineering
King Fahd University of Petroleum and Minerals
Dhahran 31261, Saudi Arabia

†Department of Electrical and Computer Engineering
Umm Al-Qura University
Makkah, Saudi Arabia

An adaptive output feedback controller using neural networks for improving the dynamic stability of a wind turbine generator supplying an infinite bus through a transmission line under widely varying conditions is presented. The need for adaptive output feedback comes from the fact that the wind turbine operates over a range of operating points, some of which are unstable; hence, no single output feedback controller gains are sufficient for the entire operating range. Neural networks are used for on-line prediction of the suitable gains for the output controller when the operating point changes. Simulation results are included to demonstrate the performance of the proposed control scheme.

1 Introduction

The integration of wind power into utility systems is an area that is attracting growing interest (Fung et al., 1981). This interest has increased lately with the installation of several large-scale wind turbines (Randall, 1980), and extensive research and development efforts on wind turbine generator systems are currently under way. Wind turbine generators possess some special characteristics not shared by other types of generating units (Hinrichsen and Nolan, 1982); the obvious one is the variability of the source of energy.

The dynamic stability of wind turbine generators has recently been given considerable attention by several investigators (Abdel-Magid et al., 1995; Hinrichsen and Nolan, 1982; Johnson and Smith, 1976; Jorgensen et al., 1976; Rau and Prasad, 1993; Wasynczuk et al., 1981). The importance of the dynamic behavior stems from the influence it has on the ability of the units to remain in synchronism, to avoid unnecessary mechanical stresses, and to operate within the limits of their rating. These factors, in turn, have a bearing on the cost of energy produced. Another important aspect of the dynamic performance of the wind turbine generator is its effect on the dynamic stability of the system to which it is connected; the units

Manuscript received in final form on April 6, 1998.
Address correspondence to H.N. Al-Duwaish.

should not contribute to the dynamic instability of the power system. Results have indicated, however, that there may be modal frequencies that are in the range of concern for large interconnected power systems (Abdel-Magid and El-Amin, 1987). Conventional power system stabilizers (PSS) can be employed to increase the damping torque of the wind turbine generator; however, the PSS design is normally based on one operating point, and its performance away from the design operating point is, of necessity, a compromise. The limitations imposed on the effectiveness of the PSS by loading conditions can be overcome by using adaptive control techniques. Self-tuning power system stabilizers (Chandra et al., 1988; Cheng et al., 1986; Hsu and Liou, 1987) have been developed for this purpose. The major drawback of self-tuning PSS is the need of model identification in real time, which is very time consuming. To the authors' knowledge, it has never been applied to wind turbine generators.

In this paper, an adaptive output feedback controller using neural networks is proposed to enhance the dynamic stability of a wind turbine generator supplying an infinite bus through a transmission line over a wide range of operating conditions. The neural network is used to change the output feedback gains when the operating point changes. The inputs to the proposed controller are limited to the accessible states. Simulation results show the effectiveness of the proposed controller in maintaining improved dynamic performance as the loading conditions vary.

2 System Dynamic Model

The wind turbine generator used for the analysis is based on the 100 kW unit for the NASA-Lewis Research Center (Thomas et al., 1975). The unit has a two-bladed propeller on a horizontal axis with a stiff shaft and a step-up gearbox. It utilizes a synchronous generator with a static excitation system. It also utilizes a blade pitch control mechanism to regulate power. A model for a 1 MVA unit, which was extrapolated from that of the 100 kW unit (Abdel-Magid and El-Amin, 1987), is used in this paper. Figure 1 shows a schematic diagram of the system under study.

The equations describing each component of the wind turbine generator system were obtained and expressed in state space formulation as

$$\dot{x}(t) = Ax(t) + Bu(t) + Td(t), \tag{1}$$

where x is n-dimensional state vector, u is m-dimensional control force vector, d is 1-dimensional disturbance vector, A is $n \times n$ system matrix, B is $n \times m$ input matrix, and T is $n \times 1$ disturbance matrix. The detailed equations characterizing the mechanical dynamics, generator and excitor systems and blade pitch controls, leading to the state space formulation, are given in Appendices A and B; the system

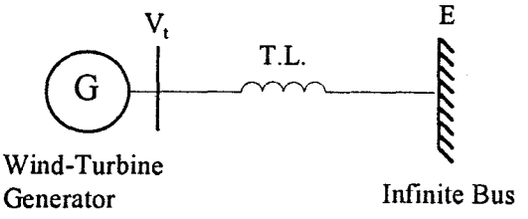

Figure 1. Schematic diagram of the system under study.

numerical data are given in Appendix C. Combining the equations describing the various components of the wind turbine generator system in state space formulation yields the system matrix A, the input matrix B, and the disturbance matrix T:

$$A = \begin{bmatrix} 0 & 377 & 0 & 0 & 0 & 0 & 0 & 0 \\ -\frac{K_1}{M} & \frac{K_\omega - D}{M} & \frac{-K_2}{M} & 0 & 0 & 0 & \frac{K_\theta}{M} & 0 \\ \frac{-K_4}{T'_{d0}} & 0 & -\frac{1}{K_3 T'_{d0}} & \frac{1}{T'_{d0}} & 0 & 0 & 0 & 0 \\ 0 & 0 & 0 & -\frac{S_E + K_E}{T_E} & \frac{1}{T_E} & 0 & 0 & 0 \\ -\frac{K_A K_5}{T_A} & 0 & -\frac{K_A K_6}{T_A} & 0 & -\frac{1}{T_A} & -\frac{K_A}{T_A} & 0 & 0 \\ -\frac{K_A K_5 K_F}{T_A T_F} & 0 & -\frac{K_A K_6 K_F}{T_A T_F} & 0 & -\frac{K_F}{T_A T_F} & -\frac{T_A + K_A K_F}{T_A T_F} & 0 & 0 \\ 0 & 0 & 0 & 0 & 0 & 0 & 0 & 1 \\ \frac{K'_\delta}{\tau_p^2} & \frac{K'_w}{\tau_p^2} & 0 & 0 & 0 & 0 & -\frac{1}{\tau_p^2} & -\frac{2\zeta}{\tau_p} \end{bmatrix},$$

$$B^T = \begin{bmatrix} 0 & 0 & 0 & 0 & \frac{K_A}{T_A} & \frac{K_A K_F}{T_A T_F} & 0 & 0 \end{bmatrix},$$

$$T^T = \begin{bmatrix} 0 & \frac{K_\nu}{M} & 0 & 0 & 0 & 0 & 0 & \frac{K'_\nu}{\tau_p^2} \end{bmatrix},$$

$$x^T = (\delta, \omega, E'_q, E_{fd}, \nu_R, \nu_3, \theta_1, \theta_2), \quad d = V_{gust}, \quad u = \nu_{ref}.$$

3 Overview of Radial Basis Functions Neural Networks

Radial basis functions neural networks (RBFNN) have been developed based on the theory of RBF approximation for real multivariable function approximation (Broomhead and Lowe, 1988). The use of RBFNN in engineering applications is increasing rabidly. RBFNN provide a powerful tool for constructing nonlinear mappings from input-output data. Moreover, RBFNN has the advantage of easy and effective learning algorithm compared with other multilayer feedforward neural networks. The attractive feature of the RBFNN lies in the linear dependence in the parameters, which greatly simplifies the design and analysis of such networks. A typical multi-input, multi-output RBFNN is shown in Figure 2, which consists of three layers: an input layer with n inputs, one hidden layer with m neurons, and

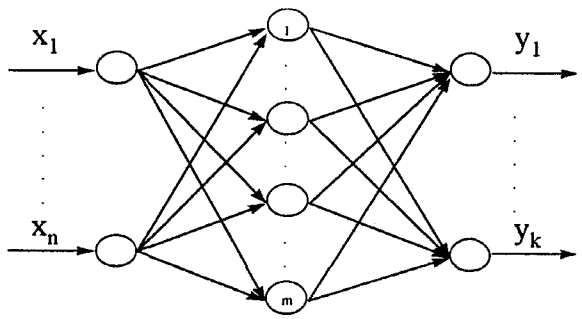

Figure 2. Radial basis function neural network.

an output layer with k output units. Each output unit in the RBFNN performs the following function:

$$y_i(x) = \sum_{j=1}^{m} w_{ij}\phi_j(x); \quad i = 1, 2, \ldots, k, \tag{2}$$

where $\phi_j(x)$'s are radially symmetric functions representing the nonlinearities in the hidden layer. The most commonly used function is the Gaussian function given by

$$\phi_j(x) = \exp\left(\frac{-(x - \hat{x}_j)^2}{2\sigma_j^2}\right). \tag{3}$$

The Gaussian function is defined by a center position $\hat{x}_j$ and a width σ_j. The center of the basis function can be determined by simple heuristic approaches, such as the k-means clustering method, and the width can be determined using nearest neighbor method (Broomhead and Lowe, 1988; Moody and Darken, 1989). The number of hidden units can be selected as the number of training patterns. This approach often leads to very large networks and poor generalization capabilities. Different approaches have been proposed for the selection of the number of hidden units (Bishop, 1991; Spect, 1990). The weights from hidden to output layers can be computed using the least mean square (LMS) or pseudo inverse methods.

4 Output Feedback Design and Simulation Results

In many practical situations, some of the system states cannot be measured. Thus, an alternative and preferred way is to feedback the measured states (outputs) that can serve as the inputs to the controller. This gives a physically realizable control system to implement. Output feedback has been used in many control applications (Lee and Wu, 1995). A survey of output feedback design approaches can be found in (Syrmos et al., 1994). Consider a linear time-invariant system described by

$$\begin{aligned} \dot{x}(t) &= Ax(t) + Bu(t), \\ y(t) &= Cx(t), \end{aligned} \tag{4}$$

where $x(t)$, $u(t)$, and $y(t)$ are the $n \times 1$ state vector, $m \times 1$ input vector, and $p \times 1$ output vector, respectively. A, B, and C are constant matrices of appropriate dimensions. The output feedback control law is given by

$$u(t) = -Gy(t). \tag{5}$$

Thus, the closed loop system is given by

$$\begin{aligned} \dot{x}(t) &= (A - BGC)x(t), \\ y(t) &= Cx(t). \end{aligned} \tag{6}$$

The problem of output feedback design is to find the output feedback gain vector G such that the eigenvalues of the closed-loop system are placed in some desired locations that guarantee stability and acceptable transient behavior. Following is an output feedback design method that places the eigenvalues of the closed loop

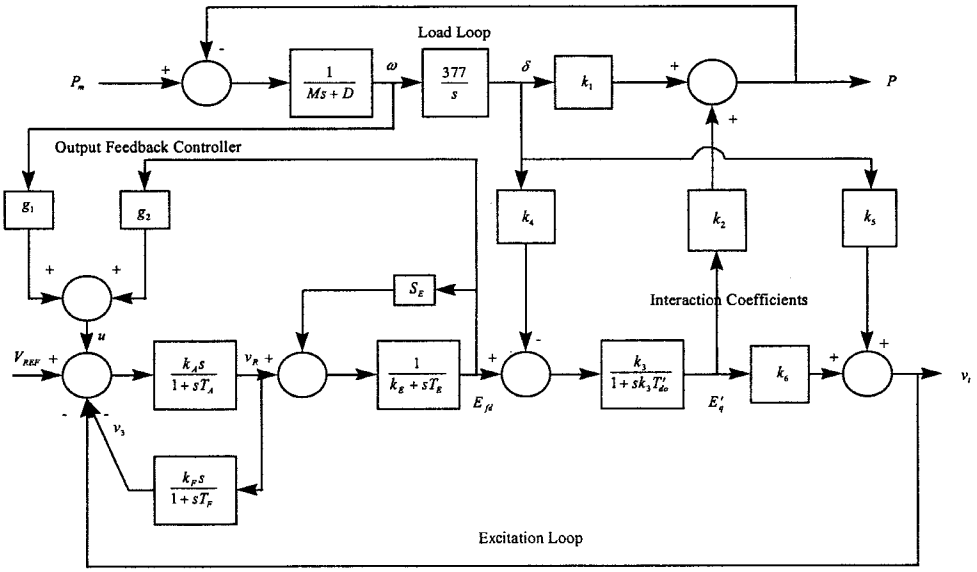

Figure 3. Block diagram of the generator-exciter model with output feedback controller.

system in a vertical strip on the real axis of the s-plane bounded by $(-h_1, -h_2)$ (Shieh et al., 1986). The output feedback gain vector G can be computed from

$$G = \mu F C^{+}. \tag{7}$$

Where C^{+} is the pseudoinverse of C, μ is selected as

$$\mu = \frac{1}{2} + \frac{h_2 - h_1}{2tr(\hat{A}^{+})} = \frac{1}{2} + \frac{h_2 - h_1}{tr(BF)}, \tag{8}$$

with $tr(\hat{A}^{+}) = \sum_{i=1}^{n} \lambda_i^{+} = \frac{1}{2} tr(BF)$ and $\lambda_i^{+} (i = 1, \ldots, n^{+})$ are the eigenvalues of $\hat{A}^{+}$ in the right half-plane of the complex s-plane, $tr(.)$ designates the trace of $(.)$:

$$F = R^{-1} B^{T} P, \tag{9}$$

where P is the positive definite symmetric matrix solution of the following Riccati equation:

$$\hat{A}^{T} P + P\hat{A} - PBR^{-1}B^{T}P = 0 \tag{10}$$

with $\hat{A} = A + h_1 I$.

The wind turbine model discussed in section 2 has two outputs, ω and E_{fd}. The output feedback controller structure is shown in Figure 3 and described by

$$u(t) = g_1 \omega + g_2 E_{fd}. \tag{11}$$

The operating point selected for the design is $(P, Q) = (1.0, -0.4)$ p.u. The eigenvalues of the system for the selected operating point are $\{-650.93, -1.70 \pm 6.37j, -4.74 \pm 4.65j, 0.12 \pm 1.82j, -1.06\}$, which indicate an unstable operating point. Following the output feedback design procedure, the output feedback gains are

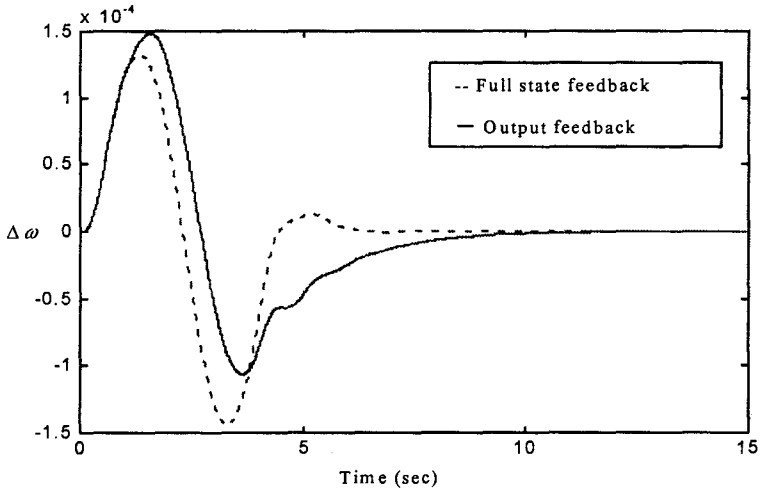

Figure 4. Frequency change with full state feedback and output feedback controllers.

$g_1 = -15.1667$ and $g_2 = 0.1899$. The eigenvalues of the system with output feedback are $\{-646.41, -1.44 \pm 6.39j, -4.74 \pm 4.65j, -4.39, -0.75 \pm 0.15j\}$. To investigate the performance of the proposed output feedback, the system illustrated in Figure 1 was simulated for a wind gust of the form (Abdel-Magid et al., 1995)

$$V_{gust} = G_u \left(1 - \cos \frac{2\pi t}{T}\right), \quad 0 < t < T. \tag{12}$$

First, output feedback controller is compared with full state feedback controller, designed using the well-known Linear Quadratic Regulator (LQR) design method (Kirk, 1970), and the results are shown in Figure 4, where comparable results are obtained. Figure 5 shows the change in frequency for the loading condition $(P, Q) =$

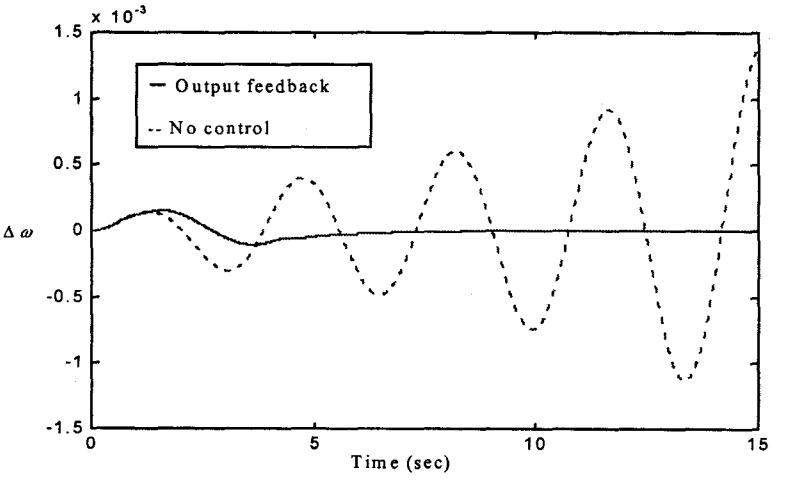

Figure 5. Frequency change with output feedback controller and no control.

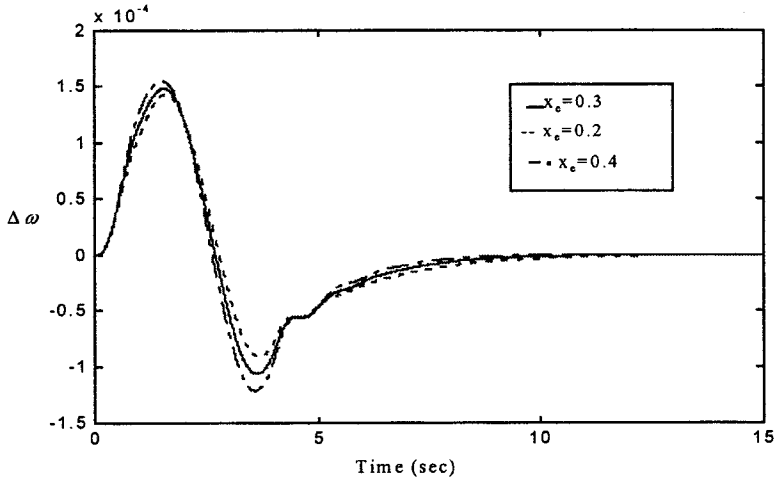

Figure 6. Effects of x_e (transmission line reactance) on frequency change.

(1.0, −0.4) p.u. with and without output feedback control. From the response, it is shown that the output feedback clearly stabilizes the system and improves the transient behavior.

To test the performance of the output feedback controller, various loading conditions and parameter values were assumed and the response of the system for the same wind gust disturbance were studied. Figures 6, 7, and 8 show the effects of varying the transmission line reactance, x_e, the open circuit field time constant, T'_{do}, and the rated wind speed, V, on the system response, which clearly indicate the robustness of the output feedback controller to parameter variations. Figure 9 shows the effects of changing the operating point on the controller performance. Although the performance of the output feedback controller is acceptable for dif-

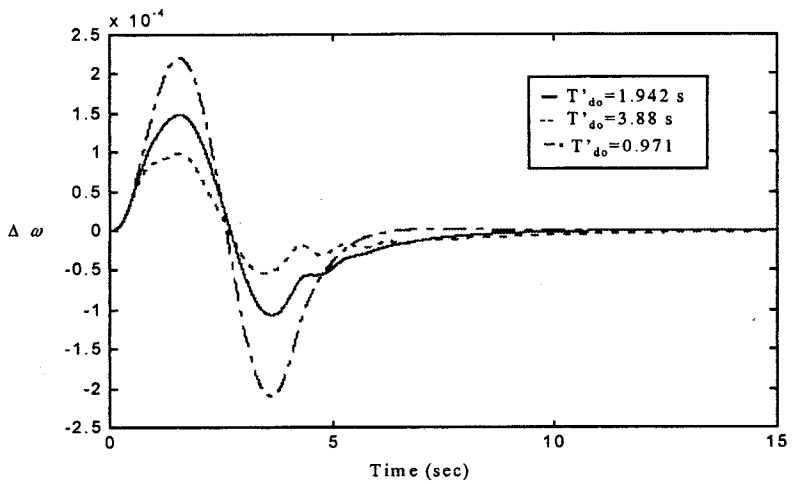

Figure 7. Effects of T'_{do} (open circuit field time constant) on frequency change.

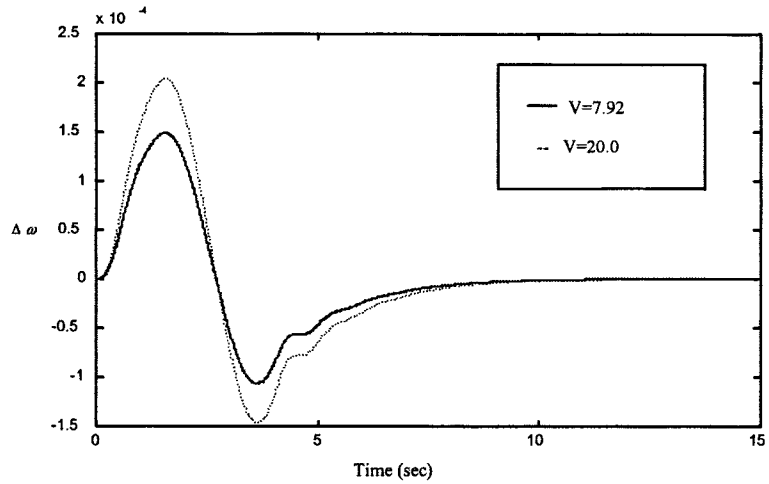

Figure 8. Effects of V (rated wind speed) on frequency change.

ferent operating points, the performance can be improved greatly by introducing an adaptive output feedback where the output feedback gains are changed at any operating point.

5 Adaptive Output Feedback

The need for adaptive output feedback controller comes from the fact that the wind turbine discussed in section 2 operates over a range of operating points, some of which are unstable. Thus, no single output feedback controller is sufficient for the entire operation. In the adaptive output feedback controller, a neural network with inputs P and Q is used to generate the output feedback gains (g_1 and g_2) in Figure 3. When the operating point changes, the RBFNN will produce new out-

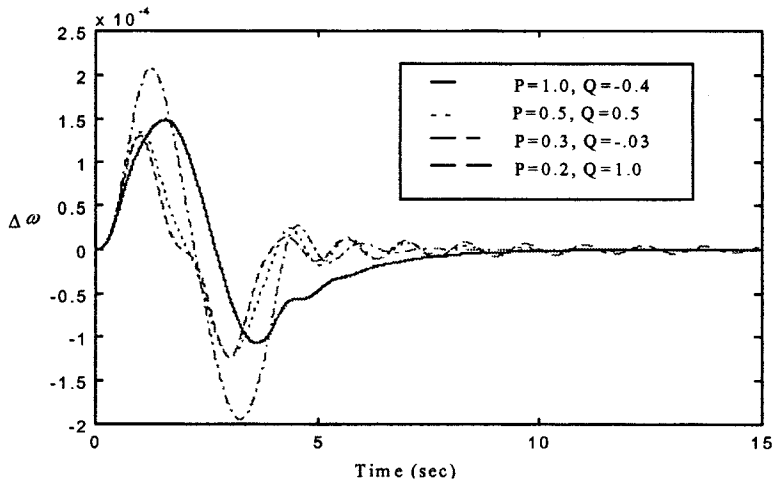

Figure 9. Frequency change for various loading conditions.

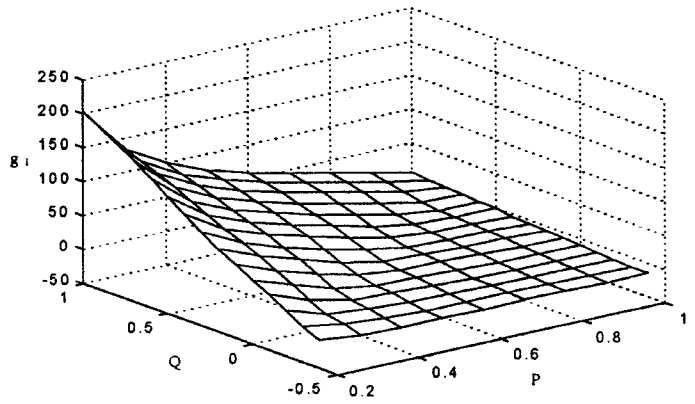

Figure 10. Change of output feedback gain g_1 for different operating points.

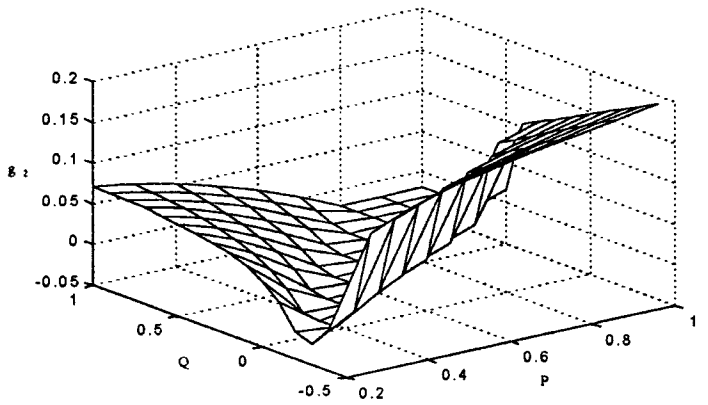

Figure 11. Change of output feedback gain g_2 for different operating points.

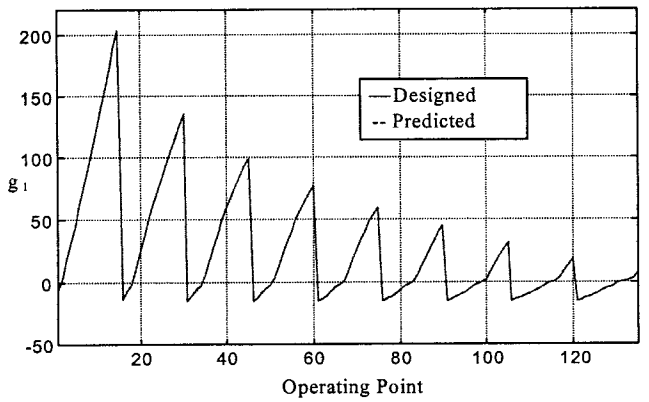

Figure 12. Designed and predicted output feedback gain g_1.

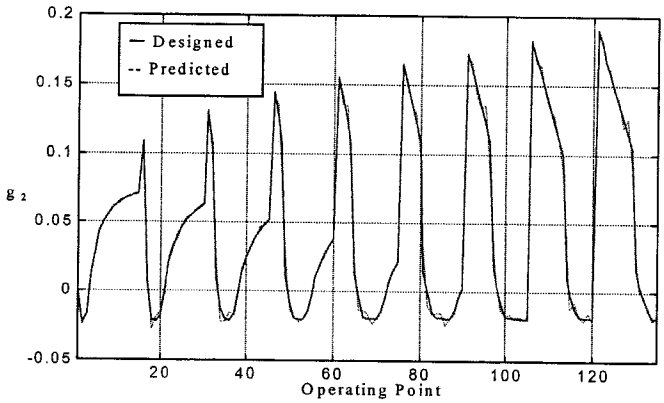

Figure 13. Designed and predicted output feedback gain g_2.

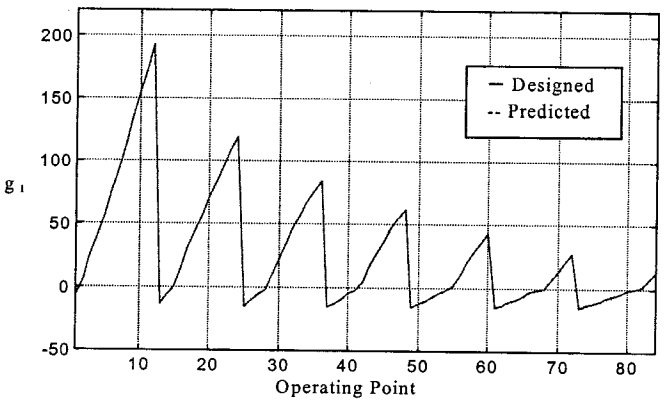

Figure 14. Designed and predicted output feedback gain g_1.

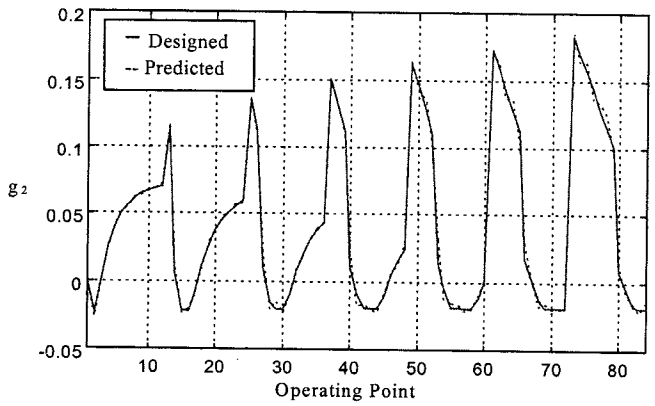

Figure 15. Designed and predicted output feedback gain g_2.

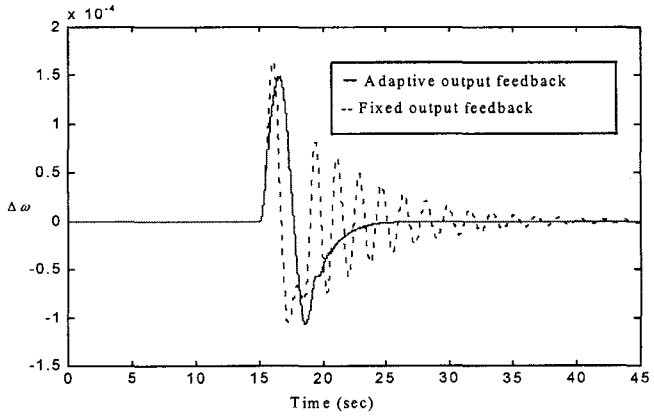

Figure 16. Frequency change when the operating point changes from $(1, -0.4)$ to $(0.2, 1)$ with fixed output feedback and adaptive output feedback controllers.

put feedback gains suitable for the new operating point. The RBFNN is used to model the nonlinear relationships (shown in Figures 10 and 11) between operating points and output feedback gains. To train the neural network, 135 operating points generated by changing P from 0.2 to 1.0 and Q from -0.5 to 1 in steps of 0.1, which represent the practical operating range of the wind turbine generator, are used. For each operating point, output feedback gains g_1 and g_2 are calculated as described in section 4. The RBFNN used has two inputs (P, Q), two outputs (g_1, g_2), and 30 neurons in the hidden layer. The results of the training are shown in Figures 12 and 13, which indicate good agreement between the actual feedback gains and outputs of the neural network. To test the generalization capabilities of the neural network, 85 operating points (different from training operating points) are used. The results of the test are depicted in Figures 14 and 15, which show that the network is able to predict the output feedback gains for new operating points. To test the performance of the adaptive output feedback controller, a comparison between adaptive and fixed output feedback controller is shown in Figure 16 when the operating point changes from $(1, -0.4)$ to $(0.2, 1)$. It can be seen that the adaptive output feedback controller outperforms the fixed output controller in damping the system oscillations. This demonstrates that the adaptive feedback controller is very suitable for on-line stabilization of wind turbine generators.

6 Conclusion

In this paper, an adaptive output feedback control scheme using radial basis neural networks is developed for a wind turbine generator supplying an infinite bus through a transmission line. The inputs to the controller are restricted to the accessible states only, which allows for practical implementation. The radial basis function neural networks are used to predict the suitable output feedback gains for any operating point. The use of adaptive output feedback is motivated by the fact that the wind turbine generator operates over a wide range of operating conditions, and hence no single output feedback gains are sufficient for the entire operation. Simulation results indicate that fixed output feedback can perform satisfactorily for practical

ranges of parameter variations and for many operating points, but the controller performance can be improved greatly by the use of adaptive output feedback gains.

Acknowledgment

The authors would like to acknowledge the support of their respective universities.

References

[1] Abdel-Magid, Y. L., Al-Hamouz, Z. M., and Bakhashwain, J. M., 1995, A variable-structure stabilizer for wind turbine generators, *Electric Power Systems Research*, Vol. 33, pp. 41–48.

[2] Abdel-Magid, Y. L., and El-Amin, I. M., 1987, Dynamic stability of wind-turbine generators under widely varying loading conditions, *Electr. Power Energy Syst.*, Vol. 9, pp. 180–188.

[3] Bishop, C., 1991, Improving the generalization properties of radial basis function neural networks, *Neural Computation*, Vol. 3, pp. 579–588.

[4] Broomhead, D. S., and Lowe, D., 1988, Multivariable functional interpolation and adaptive networks, *Complex Systems*, Vol. 2, pp. 321–355.

[5] Chandra, A., Malik, O. P., and Hope, G. S., 1988, A self-tuning control for the control of multi-machine power systems, *IEEE Trans. PWRS*, Vol. 3, pp. 1065–1071.

[6] Cheng, S. J., Chow, Y. S., Malik, O. P., and Hope, G. S., 1986, An adaptive synchronous machine stabilizer, *IEEE Trans. PWRS*, Vol. 1, pp. 101–109.

[7] DeMello, F. P., and Concordia, C., 1969, Concepts of synchronous machine stability as affected by excitation system control, *IEEE Trans. PAS*, Vol. 88, pp. 316–329.

[8] Fung, K. T., Scheffler, R. L., and Stolpe, J., 1981, Wind energy- utility perspective, *IEEE Trans. PAS*, Vol. 100, pp. 1176–1182.

[9] Hinrichsen, E. N., and Nolan, P. J., 1982, Dynamics and stability of wind turbine generators, *IEEE Trans. PAS*, Vol. 101, pp. 2640–2648.

[10] Hsu, Y. Y., and Liou, K. L., 1987, Design of self-tuning PID power system stabilizers for synchronous generators, *IEEE Trans. EC*, Vol. 2, pp. 343–348.

[11] Hwang, H. H., and Gilber, L. J., 1978, Synchronization of wind turbine generators against an infinite bus under gusting wind conditions, *IEEE Trans. PAS*, Vol. 97, pp. 536–544.

[12] Johnson, C. C., and Smith, R. T., 1976, Dynamics of wind generators on electric utility networks, *IEEE Trans. AES*, Vol. 12, pp. 483–492.

[13] Jorgensen, G. E., Lotker, M., Meier, R. C., and Brierley, D., 1976, Design, economic and system considerations of large wind driven generators, *IEEE Trans. PAS*, Vol. 95, pp. 870–878.

[14] Kirk, D. E., 1970, *Optimal Control Theory*, Prentice-Hall.

[15] Lee, Y., and Wu, C., 1995, Damping of power system oscillations with output feedback and strip eigenvalues assignment, *IEEE Trans. On Power Systems*, Vol. 10, No. 3, pp. 1620–1626.

[16] Moody, J., and Darken, C. J., 1989, Fast learning in networks of locally turned processing units, *Neural Computation*, Vol. 1, pp. 281–294.

[17] Pantalone, D. K., and Fouad, A. A., 1978, Modes of oscillations of wind generators in large power systems, IEEE PES Summer Meet., Los Angeles, CA, Paper No. A 78 579-5.

[18] Qazi, A. Q., and Ramakumar, R., 1977, Behavior of wind driven synchronous generators under wind guests, IEEE Conf. Control of Power Systems, College Station, TX, pp. 20–25.

[19] Randall, P., 1980, *Wind Power-Bibliography*, Institution of Electrical Engineers, London.

[20] Rau, V. G., and Durga Prasad, G., 1993, Dynamic stability assessment of wind turbine generators using the Lyapunov function approach, *Electric Power Systems Research*, Vol. 27, pp. 61–72.

[21] Shieh, L. S., Dib, H. M., and Mcinnis, B. C., 1986, Linear quadratic regulators with eigenvalue placement in a vertical strip, *IEEE Trans. On AC*, Vol. 31, No. 3, pp. 241–243.

[22] Spect, D. F., 1990, Probabilistic neural networks, *Neural Computation*, Vol. 3, pp. 109–118.

[23] Syrmos, V. L., Abdullah, C., and Dorato, P., 1994, Static output feedback: A survey, *Proceedings of the 33rd Conference on Decision and Control*, Lake Buena Vista, FL, pp. 837–842.

[24] Thomas, R., Puthoff, R., Savino, J., and Johnson, W., 1975, Plans and status of the NASA-Lewis Research Center wind energy projects, Joint IEEE/ASME Power Conf., Portland, OR, Paper No. NTIS N75-21795.

[25] Wasynczuk, O., Man, D. T., and Sullivan, J. P., 1981, Dynamic behaviour of a class of wind turbine generators during random wind fluctuation, *IEEE Trans. PAS*, Vol. 100, pp. 2837–2845.

Appendix A

Linearized Small-Perturbation Model of a Synchronous Generator

The equations describing the steady state operation of a synchronous generator connected to an infinite busbar through an external reactance can be linearized about any particular operating point and reduced to equations (A1)–(A3) below (DeMello and Concordia, 1969). All variables are evaluated at their predisturbance steady state operating point from known values of ν_{t0}, P_0, and Q_0, as given in equations (A4)–(A8). All variables preceded by Δ are deviations of these variables from their values at the steady state operating point. The constants $K_1, \ldots, K_6$ are given in equations (A9)–(A14).

$$\Delta P_m - \Delta P = M\frac{d^2\delta}{dt^2}, \quad \Delta P = K_1\Delta\delta + K_2\Delta E'_q, \tag{A1}$$

$$\Delta E'_q = \frac{K_3}{1 + sT'_{d0}K_3}\Delta E_{fd} - \frac{K_3K_4}{1 + sT'_{d0}K_3}\Delta\delta, \tag{A2}$$

$$\Delta\nu_t = K_5\Delta\delta + K_6\Delta E'_q, \tag{A3}$$

$$i_{q0} = \frac{P_0\nu_{t0}}{[(P_0x_q)^2 + (\nu_{to}^2 + Q_0x_q)^2]^{1/2}}, \quad i_{d0} = \frac{Q_0 + x_qi_{q0}^2}{\nu_{q0}}, \tag{A4}$$

$$\nu_{d0} = i_{q0}x_q, \quad \nu_{q0} = (\nu_{to}^2 - \nu_{d0}^2)^{1/2}, \tag{A5}$$

$$E_{q0} = \nu_{q0} + i_{d0}x_q, \tag{A6}$$

$$E_0 = [(\nu_{d0} + x_ei_{q0})^2 + (\nu_{q0} - x_ei_{d0})^2]^{1/2}, \tag{A7}$$

$$\delta_0 = \tan^{-1}\left(\frac{\nu_{d0} + x_ei_{q0}}{\nu_{q0} - x_ei_{d0}}\right), \tag{A8}$$

$$K_1 = \frac{x_q - x'_d}{x_e + x'_d}i_{q0}E_0\sin\delta_0 + \frac{E_{q0}E_0\cos\delta_0}{x_e + x_q}, \tag{A9}$$

$$K_2 = \frac{E_0\sin\delta_0}{x_e + x'_d}, \quad K_3 = \frac{x'_d + x_e}{x_d + x_e},$$

$$K_4 = \frac{x_d - x'_d}{x_e + x'_d} E_0 \sin\delta_0, \tag{A10}$$

$$K_5 = \frac{x_q}{x_e + x_q}\frac{\nu_{d0}}{\nu_{t0}} E_0 \cos\delta_0 - \frac{x'_d}{x_e + x'_d}\frac{\nu_{q0}}{\nu_{t0}} E_0 \sin\delta_0,$$

$$K_6 = \frac{x_e}{x_e + x'_d}\frac{\nu_{q0}}{\nu_{t0}}. \tag{A11}$$

The linear state space equations for the exciter model are as follows:

$$\dot{\nu}_R = \frac{K_A}{T_A}\nu_{ref} - \frac{K_A}{T_A}\nu_t - \frac{K_A}{T_A}\nu_3 - \frac{1}{T_A}\nu_R, \tag{A12}$$

$$\dot{\nu}_3 = \frac{K_F K_A}{T_F T_A}(\nu_{ref} - \nu_t) - \left(\frac{K_F K_A}{T_F T_A} + \frac{1}{T_A}\right)\nu_3 - \frac{K_F}{T_F T_A}\nu_R, \tag{A13}$$

$$\dot{E}_{fd} = \frac{1}{T_E}\nu_R - \left(\frac{K_E + S_E}{T_E}\right) E_{fd}. \tag{A14}$$

Appendix B

Wind Machine Equations

The turbine is usually represented by a nonlinear wind power model relating power output to wind speed and power coefficient:

$$P_m = \frac{1}{2}\rho a V^3 C(\theta, \lambda), \tag{B1}$$

where P_m is mechanical load, a is area swept by blades, V is wind speed, $C(\theta, \lambda)$ is power coefficient, θ is blade pitch angle, ρ is air density, and λ is ratio of tip speed to wind speed. The power coefficient is a function of blade angle and the ratio of tip speed to wind speed. This relation is usually provided by the manufacturer in the form of a set of nondimensional curves. (Wasynczuk et al., 1981) documents such a set for the NASA-Lewis 100 kW unit. The curves could be used to derive a linearized expression of the mechanical torque in p.u., as a function of the electrical rotational speed, the blade pitch angle, and the wing speed in the form

$$T_m = K_V V + K_\theta \theta + K_\omega \omega, \tag{B2}$$

where T_m is mechanical torque (p.u.), ω electrical speed (p.u.), K_V coefficient of torque from wind speed $K_V = dT_m/dV$, K_0 coefficient of torque from pitch angle, $K_\theta = dT_m/d\theta$, K_ω coefficient of torque from rotational speed, $K_\omega = dT_m/d\omega$, and all variables are derivations from the initial operating points. Numerical values for the constants K_ω, K_θ, and K_V were obtained from (Abdel-Magid et al., 1987). The 1 MVA unit modeled here will attempt to regulate the speed and its integral during normal operation. This is equivalent to speed regulation and an apparent form of power regulation. The later could be obtained by changing the pitch angle as a function of speed. Modeling the pitch blade controls by a second-order system (Hwang and Gilber, 1978), the following equation is obtained:

$$\tau_p^2 \frac{d^2\theta(t)}{dt^2} + 2\zeta\tau_p \frac{d\theta(t)}{dt} + \theta(t) = K'_\omega \omega + K'_V V + K'_\delta \delta, \tag{B3}$$

where τ_p is actuator time constant, ζ is damping ratio, and K'_ω, K'_V, K'_δ are pitch angle regulation constants. The two states θ_1 and θ_2 are obtained by transforming the second-order differential equation given by (B3) into two first-order state equations.

Appendix C

System Data

The system data used in the design and analysis are as follows:

Generator (Hwang and Gilber, 1978):

$$x_d = 2.21, \quad x'_d = 0.165, \quad x_q = 1.064 \text{ p.u.}, \quad M = 19.04 \text{ s},$$
$$D = 0, \quad \omega_0 = 377 \text{ rad/s} \quad T'_{d0} = 1.942 \text{ s}, \quad \nu_{t0} = 1.0 \text{ p.u.}$$

Transmission line:

$$x_e = 0.3 \text{ p.u.}$$

Excitation system (Pantalone and Fouad, 1978):

$$K_A = 400, \quad T_A = 0.02 \text{ s}, \quad K_E = 1, T_E = 1.3 \text{ s},$$
$$K_F = 0.03, \quad T_F = 1 \text{ s}, \quad S_E = 0.64.$$

Pitch angle control parameters (Pantalone and Fouad, 1978):

$$K'_V = -0.337, \quad K'_\omega = -20.94, \quad K'_\delta = -0.0055,$$
$$\tau_p = 0.15 \text{ s}, \quad \zeta = 0.707.$$

Aerodynamic parameters (Pantalone and Fouad, 1978):

$$K_\omega = -3.3, \quad K_\theta = 0.118, \quad K_V = 0.337.$$

Rated wind speed:

$$V = 7.92 \text{ m/s}.$$

Wind gust disturbance:

$$T = 4 \text{ s}, G_u = 7.5\%.$$